A CLOSED-FORM EXPRESSION FOR REPRESENTING THE DISTRIBUTED NATURE OF THE SPIRAL INDUCTOR

David M. Krafcsik and Dale E. Dawson

Westinghouse Electric Company
P.O. Box 1521, MS 3902
Baltimore, Md. 21203

ABSTRACT

A closed form expression for the modeling of rectangular spiral inductors to twice the self-resonant frequency is derived and compared to experimental results. The mutual inductance effects of the ground plane, and phase shift effects are considered in this analysis.

INTRODUCTION

The departure of the spiral inductor from lumped element behavior complicates its use in MMIC applications. By "unwinding" the spiral, it can be seen that the electrical length of the spiral will be significant at high frequencies where the total length approaches a quarter wavelength, and the point is reached where the spiral is self-resonant. As a result of this electrical length, the inside turns have progressively greater phase lag relative to the outside turns. This causes the values of inductance and shunt capacitance in the equivalent lumped-pi model to have a natural variation with frequency. This variation of inductance and capacitance with frequency makes the standard pi-model equivalent circuit with its frequency independant elements inherently inappropriate to represent the spiral inductor. Table 1 shows a lumped pi model which is used to represent a spiral inductor across a wide band of frequencies. Notice that the lumped pi elements change 20-50% as frequency is increased. This equivalent circuit was generated using the techniques that follow.

An approach is now described that accounts for both the proximity of the ground plane and the coil electrical length out to twice the self-resonant frequency of the coil. This approach uses closed form equations for inductance and capacitance, and advantage is taken of the inherently fast computational speed to compute a pi-model at each frequency. Two-port parameters then are computed from each pi-model to accurately represent the coil at each frequency. Thus, the computations can be included in a subroutine which gives the low frequency-inductance of the coil but otherwise directly represents the coil by two-port s-parameters without the limitations of one frequency independant, pi-model to represent the coil for all the frequencies of interest. Experimental results are given which agree with the closed-form calculations within 5% out to frequencies as high as the self-resonant frequency, and 10% agreement was found out to twice the self-resonant frequency.

THE APPROACH

Grover's equations [1] give mutual inductance between elemental line segments. These elemental relations were used by Greenhouse [2] on each segment of a square spiral inductor to compute the total inductance of the spiral including the negative mutual inductance between segments on opposite sides of the coil. The ideal case of the inductor in free space with no ground plane present was considered in the analysis by Greenhouse. The elemental relations of Grover are used in this approach the same way as they are used by Greenhouse, but two additional effects are included. The first is the lowering of the inductance by the presence of a ground plane, compared to the inductance without a ground plane present, as calculated by Greenhouse. The ground plane lowers the inductance by typically 20% when the spiral diameter is large compared to the ground plane distance. To account for the ground plane, the image of the spiral in the ground plane (figure 1) is used as a basis for applying Grover's elemental relations to each segment of the image spiral as well as the topside spiral. The image, which is located at twice the substrate thickness from the actual spiral, contributes a net negative mutual inductance because the current flow is in the opposite direction in the return path.

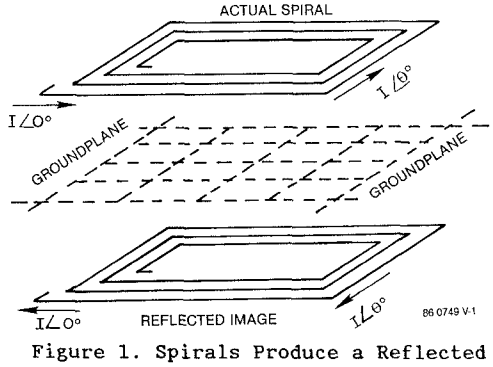

Figure 1. Spirals Produce a Reflected Image in the Ground Plane

The second effect is that of propagation delay around the spiral. Again, Grover's elemental relations are used to compute the mutual inductance between each segment of the spiral and its image in the groundplane, with the

phase difference between the currents in each segment being accounted for by vectorially adding the mutual inductances. If one assumes unit current injected in one end of the spiral, then the induced voltages in each segment have progressively more phase lag around the spiral relative to the first segment. Figure 2 shows the equivalent of two segments separated by a delay. The two segments have self-inductances L1 and L2 and a mutual inductance M. The loop equation shows that the self-inductances add directly and the mutuals add vectorially, where the effective inductance is M*cos(θ) for each component of mutual inductance. Thus, at higher frequencies the mutual inductance adds progressively less and even subtracts from the self-inductance terms. The relationship of figure 2 allows the vector sum of all the mutuals to be taken to arrive at the total inductance of the coil. Therefore, the mutual coupling of each segment to itself and every other segment is accounted for in the presence of the phase shift around the coil.

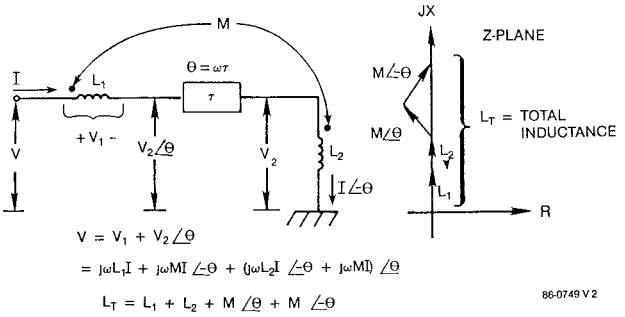

Figure 2. The Effect of Phase Shift on the Total Inductance of the Coil

Even and odd-mode capacitances of the coil are computed from the capacitances of infinite and semi-infinite arrays of strips using Smith's [3] fast converging algorithms. The outside and inside turns have greater capacitances per unit length, in even mode, because the fringing fields spread out over a larger distance. In this case the capacitance of an edge-most strip in a semi-infinite array is used. In the case of a middle strip, the even and odd-mode capacitances of a strip in the infinite array are used. Then the capacitance of each segment is computed in the following manner. Using the total length of the coil as a basis, the capacitance values of all the segments that constitute one-half of the coil length are lumped into one of the shunt capacitors in the pi-model, and the capacitance of all the segments of the remaining half are lumped into the other capacitor in the pi-model. These resulting capacitance values in the pi-model are not symmetric. The outside turn has the most periphery with fringing and is the side of the coil connected with the larger of the two capacitors in the pi-model for all practical frequencies. At very high frequencies the reverse may be true, but only at several times the self-resonant frequency, where individual pairs of turns are approaching the odd-mode case.

Now, both the capacitance values of the pi-model change with frequency because the even and odd-mode capacitances of each segment change the loading on the coil as the phase shift around the coil varies with frequency. The frequency dependence starts at low frequency with $V_1=V_2=V_3$ in figure 3 and therefore the low frequency coil capacitance is the sum of the even-mode capacitances of each segment. As the frequency is increased, V_1 no longer equals V_2 and V_3 because of phase shift around the one turn and the odd-mode contribution increases the effective capacitance. The capacitive reactance to ground for a particular segment then is computed as:

$$X_c = V_1 / (| Ie+Io_1+Io_2|).$$

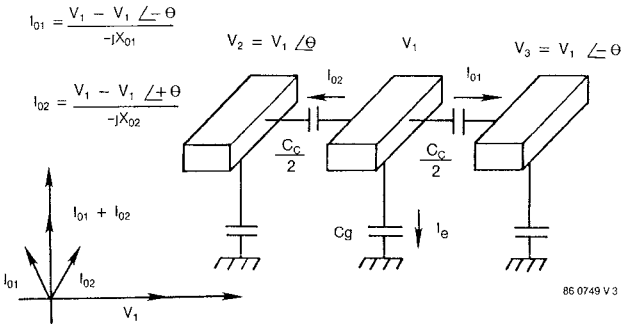

Figure 3. The Effect of Phase Shift on the Effective Capacitance to Ground of the Spiral

MODELING DETAILS

The following assumptions are made to complete the description of the modeling approach:

1) The coil is divided up into discrete straight line segments. In the case of a rectangular spiral each side of the spiral is a segment. Polygon-shaped and circular coil geometries also can be analyzed by this technique by subdivision into the appropriate number of segments, and by using another of Grover's formulations which allows for nonparallel line segments;

2) The phase shift along each segment is zero. The phase shift between segments is computed using the path length around the coil between the centers of each segment, along with the propagation velocity determined from the effective dielectric constant for the microstrip formed from the segment width;

3) The phase lag around three or more sides of the coil is greater than the phase lag directly across the coil. Using closed-form mutual inductance equations assume the fields are not delayed in time even though there may be phase differences between the currents giving rise to the fields. With the current constrained to flow around the turns of the spiral, the field delay across the coil is less than the delay due to the path length around the coil;

4) Since a full nodal network analysis based on series and shunt currents for each segment is not being used, an equivalent capacitance to ground is computed by taking the magnitude of the sum of the capacitive current vectors, Ie, Io_1, and Io_2 as shown in figure 3. This approximation is helped in that V_1 and V_2/V_3 are the voltages across one turn and not the voltage across the entire coil.

COMPARISON OF MODELED AND MEASURED RESULTS

Two square spirals, shown in figure 4, differing in size by 2:1 were analyzed and tested and the results compared. Inductor A had a diameter of 400μm, a 20um line width, and a 10μm gap. It was fabricated on GaAs by the metal liftoff technique with .75μm thick evaporated gold metallization. Inductor B was fabricated by the same technique on GaAs with a much larger diameter of 715μm, a 20μm line and gap width, and 1.3μm thick gold. The substrate thicknesses were 100μm and 250μm respectively (4 and 10 mils). The calculated s-parameters are shown in table 2 along with the measured s-parameters. S11 and S22 go through resonance at 5.0 and 5.5 GHz respectively on inductor A (table 2A) on both calculated and measured, within 3 degrees. No optimization was done on either set of s-parameters. The calculated s-parameters are as computed from the closed-form expressions. The results of inductor B of larger size are in table 2B. S11 and S22 resonances in both the measured and calculated results likewise agree within 5%. The calculated angles of all the s-parameters in both cases compare to the measured within 3 degrees up to self-resonance. Calculated |S21| was within 5% up to self-resonance and within 10% up to twice resonance when compared to the measured |S21|.

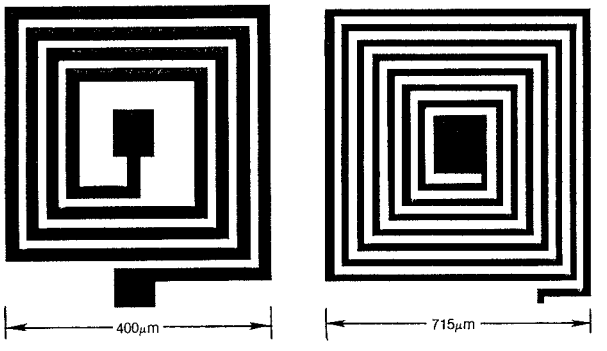

Figure 4. Spiral Inductor Model Program Is Tested on Two Different Size Spirals

SOME EXAMPLE CALCULATIONS

All of the inductance calculations performed in this paper are based on three equations, all from Grover. The first is the expression for the mutual inductance between two parallel filamentary current conductors of length L(cm) and distance D(cm) apart.

where M is the mutual inductance in nano-Henries. This equation applies directly only to cases where the cross-sectional dimensions of the two lines are small compared to the distances separating them, such as in the case of the mutual inductance between a topside spiral segment and its ground plane reflection. For two conductors which are closely spaced, such as two adjacent topside spiral segments, a Geometric Mean Distance (GMD) must be calculated and used in place of the center-to-center distance. The following formula gives the GMD for two parallel line segments of rectangular cross-section which are relatively thin compared to their width:

$$M = 2L\left[\log_e\left(\frac{L}{D}+\sqrt{1+\frac{L^2}{D^2}}\right)-\sqrt{1+\frac{D^2}{L^2}}+\frac{D}{L}\right] \qquad (1)$$

where D is the center-to-center distance.

Third, the GMD of a rectangular cross-section wire to itself may be approximated by the following formula:

$$GMD = EXP\left[\log_e(D)-\left(\frac{1}{12\left(\frac{D}{W}\right)^2}+\frac{1}{60\left(\frac{D}{W}\right)^4}+\frac{1}{168\left(\frac{D}{W}\right)^6}+\right)\right] \qquad (2)$$

$$GMD = .2235\ (W + T) \qquad (3)$$

where GMD is in the same units as width and thickness.

These three formulas have been used to predict precisely the static inductances of a wide variety of microstrip transmission line structures which are composed of only parallel or perpendicular line segments.

To illustrate their use more clearly, these equations are applied to inductor B (depicted in figure 4) as follows. First the self inductances of each straight line segment are computed, and for the first segment in inductor B the length is 705μm and the width and thickness are 20μm and 1μm respectively. So,

$$GMD = .2235\ (W+T) = .2235(20+1) = 4.6935\mu m$$

and using L=705μm and D=4.6935μm in eqn. #1 we calculate:

$$\text{Self Ind} = \text{eqn. \#1 (L, D)} = .8063\ nH$$

which is the self inductance of segment #1. If the self inductances of all the other segments are calculated in a similar manner and added up, the resulting sum is 10.93 nH.

Next, the mutual inductances between the topside segments are calculated, using the first and fifth segments counting from the outside as an example. Since the segments are of different lengths, equation #1 must be applied twice as shown, where L1 and L5 are the lengths of the 1st and 5th segments, and M the resulting mutual inductance between them. We first calculate two partial values of mutual inductance using GMD from eqn. #2:

L1 = 705μm L5 = 655μm

GMD = eqn #2(W,D) where W=20μm D=40μm
= 38.90μm

M_1 = eqn #1 (L,D) where L=(L1+L5)/2=680μm
= .3550 nH D=GMD=38.9μm

M_2 = eqn #1 (L,D) where L=(L1 - L5)/2=25μm
= .00156 nH D=GMD=38.9μm

$M = M_1 - M_2 = .3535$ nH

Similarly the mutuals between each other pair of segments in the topside spiral are calculated. For the given 7 turn (28 segment) coil, there are a total of 84 positive mutual inductances and 196 negative mutual inductances to be calculated for the topside spiral alone. Hence only the totals for each will be given:

Positive Mutual Topside = 22.18 nH
Negative Mutual Topside = 7.73 nH

Note that each mutual inductance that is calculated for each pair of segments is added twice to arrive at this total, since the mutual will add to both line segments.

In a similar fashion, the mutual inductance from the topside coil to its groundplane reflection also can be calculated. The groundplane reflection is treated as if it were another physical spiral, of the same exact dimensions as the actual spiral, but located at twice the substrate thickness distant, and with currents flowing in the opposite direction. The same formulas used to calculate mutual inductance between the topside segments also are used here, with the exception that the GMD need not be computed, since the segments are so widely separated. The negative mutual inductance to the groundplane reflection, consisting of the mutual inductance between 196 pairs of lines, is calculated to be 7.27 nH for the given spiral. Likewise, the positive mutual inductance to the groundplane reflection also consists of adding the mutuals between 196 pairs of lines, though they are further apart, and the result is a smaller value of positive mutual inductance due to the groundplane reflection: 5.42 nH. Note that each mutual inductance in this case is only counted once, since the reflected spiral is not in series with the topside spiral.

To get the total low frequency inductance, we sum all the inductance totals which were calculated previously:

Total = 10.93 + 22.18 + 5.42 - 7.73 - 7.27
= 23.52 nH total inductance

If the effects of the groundplane had been neglected, then terms 3 and 5 would have dropped out, with the resulting inductance having been 25.38 nH, a 7.9% error. For the same size spiral on a 4 mil thick (100μm) substrate, the percentage error would increase to 38%, if the groundplane effects were neglected.

As shown in table 1, the inductance also is seen to decrease radically with increasing frequency. Since the capacitive and inductive components are being treated separately in this analysis, the decrease in inductance is not due to the coil looking more capacitive at higher frequencies. Instead the change is due purely to phase shift effects along the spiral length which cause the voltages imposed by the out of phase currents to not add directly. This is modeled by adding all the mutual inductances vectorially, with the assumption that current is unity (i.e., constant magnitude) throughout the coil. The phase shift from segment to segment may be computed by using standard formulas for effective dielectric constant to calculate the electrical length of each segment at the frequencies of interest. Examination of table 1 shows the phase shift has a marked effect on the total perceived inductance, causing it to decrease 25% in this case at twice the resonant frequency.

Capacitance calculations were accomplished by translating a FORTRAN program published by Smith [3] which uses closed form techniques to compute even and odd mode capacitances for both the cases of a center line in an infinite array of lines, and the end line in a semi-infinite array of lines. For the example inductor B, these numbers were computed to be:

In Between Turns:
Center Line--Even Mode Ground Cap = .18 pF/cm
Center Line--Odd Mode Ground Cap = 2.46 pF/cm

Innermost/Outermost Turns:
End Line--Even Mode Ground Cap = .55 pF/cm
End Line--Odd Mode Ground Cap = 1.69 pF/cm

These even and odd-mode capacitances are translated into ground and interline coupling capacitors by the simple relations:

$$C_g = C_e \qquad C_c = \frac{C_o - C_e}{2} \tag{4}$$

Finally the equivalent capacitance to ground for each segment is calculated as a function of frequency using the technique previously described. The resulting apparent changes in capacitance in the lumped pi model with change in frequency are shown in table 1.

CONCLUSION

The techniques shown in this paper provide a very accurate modeling tool for rectangular spiral inductors, and at a very low cost in computation time due to the closed form nature of the approach. Pucel stated [4] that in general a closed form approach was practical for the evaluation of low frequency inductance, but that the invariant lumped-pi equivalent circuit was an inadequate model over a wide frequency range. Here it has been shown that a lumped-pi equivalent circuit whose components all vary with frequency can, instead, be used to provide a good approximation to the spiral inductor. While the approach taken in this paper is similar to the Greenhouse/Grover approach, it also includes groundplane effects, capacitance calculations, and the effects of phase shift on inductance and capacitance values. When compared to two-dimensional field-theoretical approaches, such as [5], the computation time is much less. Thus, the technique appears optimum for Computer-Aided Design (CAD) approaches to circuit simulation, where fast computation time and accuracy are both necessary.

Table 2A. Measured and Calculated S-Parameters for Inductor A

	MEASURED								CALCULATED							
FREQ	S11		S21		S12		S22		FREQ	S11		S21		S12		S22	
GHz	Mag	Ang	Mag	Ang	Mag	Ang	Mag	Ang	GHz	Mag	Ang	Mag	Ang	Mag	Ang	Mag	Ang
0.5	.156	54.3	.936	-10.9	.936	-10.9	.155	54.9	0.5	.159	55.9	.927	-10.7	.927	-10.7	.158	56.5
1.0	.277	54.4	.907	-20.9	.906	-21.0	.277	55.5	1.0	.288	56.2	.898	-21.0	.898	-21.0	.288	57.3
1.5	.386	49.2	.867	-30.2	.867	-30.2	.388	49.8	1.5	.406	50.0	.857	-30.7	.857	-30.7	.405	51.8
2.0	.481	43.2	.823	-38.6	.823	-38.6	.484	42.6	2.0	.505	42.6	.808	-39.7	.808	-39.7	.505	44.9
2.5	.557	37.2	.779	-46.4	.779	-46.4	.561	35.6	2.5	.587	35.1	.757	-48.1	.757	-48.1	.586	38.0
3.0	.611	30.6	.741	-53.9	.741	-53.8	.615	29.4	3.0	.653	27.9	.708	-55.9	.708	-55.9	.652	31.2
3.5	.651	23.2	.706	-61.3	.706	-61.4	.653	23.5	3.5	.706	20.9	.661	-63.2	.661	-63.2	.705	24.7
4.0	.685	14.7	.669	-68.9	.670	-69.0	.688	17.2	4.0	.748	14.2	.618	-70.1	.618	-70.1	.748	18.4
4.5	.724	5.9	.631	-76.9	.630	-76.7	.729	10.6	4.5	.783	7.7	.578	-76.7	.578	-76.7	.783	12.2
5.0	.766	-1.6	.583	-84.6	.585	-84.6	.773	3.5	5.0	.812	1.4	.542	-83.1	.542	-83.1	.811	6.2
5.5	.800	-7.9	.532	-90.8	.532	-90.9	.806	-3.4	5.5	.836	-4.8	.509	-89.4	.509	-89.4	.835	.2
6.0	.825	-13.1	.499	-95.6	.499	-95.3	.828	-8.5	6.0	.856	-11.0	.478	-95.6	.478	-95.6	.855	-5.7
6.5	.841	-19.2	.485	-101.3	.485	-101.1	.850	-12.5	6.5	.873	-17.0	.450	-101.7	.450	-101.7	.872	-11.7
7.0	.855	-26.5	.456	-109.2	.458	-109.2	.871	-17.7	7.0	.887	-23.0	.424	-107.7	.424	-107.7	.887	-17.6
7.5	.864	-33.3	.409	-115.0	.409	-115.3	.877	-22.7	7.5	.900	-28.9	.399	-113.7	.399	-113.7	.900	-23.5
8.0	.879	-37.7	.382	-118.1	.380	-118.0	.885	-25.8	8.0	.912	-34.7	.375	-119.6	.375	-119.6	.911	-29.4

Table 2B. Measured and Calculated S-Parameters for Inductor B

0.25	.329	55.3	.878	-20.9	.876	-20.7	.331	56.1	0.25	.320	55.4	.871	-19.7	.871	-19.7	.320	56.1
0.50	.559	43.9	.766	-37.5	.767	-37.6	.559	45.7	0.50	.548	45.4	.767	-36.3	.767	-36.3	.548	46.8
0.75	.703	32.5	.652	-50.5	.655	-50.4	.703	35.1	0.75	.696	34.5	.657	-49.2	.657	-49.2	.696	36.6
1.00	.793	23.4	.562	-60.4	.561	-60.3	.795	26.9	1.00	.787	25.4	.563	-59.1	.563	-59.1	.787	28.3
1.25	.849	15.8	.484	-68.3	.485	-68.8	.851	20.1	1.25	.844	17.7	.489	-67.1	.489	-67.1	.844	21.4
1.50	.887	9.1	.425	-75.3	.422	-75.3	.889	14.0	1.50	.881	11.0	.431	-73.8	.431	-73.8	.881	15.6
1.75	.914	3.3	.377	-81.1	.376	-81.2	.916	8.8	1.75	.905	4.9	.386	-79.8	.386	-79.8	.905	10.4
2.00	.934	-1.8	.337	-86.4	.338	-86.4	.935	4.1	2.00	.923	-.9	.349	-85.3	.349	-85.3	.923	5.6
2.25	.948	-6.5	.308	-90.9	.307	-91.2	.949	-.1	2.25	.935	-6.5	.320	-90.6	.320	-90.6	.935	1.0
2.50	.953	-11.0	.281	-96.1	.282	-96.2	.962	-4.5	2.50	.945	-11.9	.296	-95.7	.296	-95.7	.944	-3.6
2.75	.962	-15.8	.260	-100.6	.258	-100.7	.963	-8.5	2.75	.952	-17.4	.276	-100.7	.276	-100.7	.952	-8.1
3.00	.957	-20.7	.242	-105.4	.243	-105.7	.963	-12.6	3.00	.958	-22.8	.259	-105.8	.259	-105.8	.957	-12.6
3.25	.957	-25.4	.232	-109.6	.232	-109.7	.965	-16.1	3.25	.962	-28.3	.244	-110.8	.244	-110.8	.962	-17.2
3.50	.955	-30.7	.224	-114.4	.224	-114.0	.960	-20.0	3.50	.966	-33.8	.231	-115.9	.231	-115.9	.965	-21.8
3.75	.951	-36.3	.218	-118.9	.217	-119.0	.958	-24.0	3.75	.969	-39.3	.220	-121.1	.220	-121.1	.968	-26.5
4.00	.945	-42.5	.219	-125.2	.219	-124.4	.954	-28.1	4.00	.971	-44.7	.210	-126.2	.210	-126.2	.971	-31.3

Table 1. Calculated Pi-Model Shows a Natural Variation With Frequency

	INDUCTOR B			
FREQ.	C1-pF	R-OHM	L-nH	C2-pF
.25 ghz	.219	9.22	23.58	.148
.50 ghz	.225	9.42	23.51	.152
.75 ghz	.233	9.62	23.41	.158
1.00 ghz	.244	9.82	23.26	.166
1.25 ghz	.255	10.02	23.08	.176
1.50 ghz	.269	10.22	22.85	.186
1.75 ghz	.283	10.41	22.59	.198
2.00 ghz	.297	10.60	22.29	.210
2.25 ghz	.312	10.79	21.95	.223
2.50 ghz	.328	10.98	21.58	.236
2.75 ghz	.343	11.17	21.18	.250
3.00 ghz	.359	11.36	20.75	.264
3.25 ghz	.376	11.54	20.30	.278
3.50 ghz	.392	11.72	19.82	.293
3.75 ghz	.409	11.91	19.32	.307
4.00 ghz	.425	12.09	18.80	.322

REFERENCES

[1]. F.W. Grover, Inductance Calculations, Van Nostrand, Princeton, N.J., 1946. Reprinted by Dover Publications 1962, pp. 17-47.

[2]. H.M. Greenhouse, "Design of Planar Rectangular Microelectronic Inductors", IEEE Transactions on Parts, Hybrids, Packaging., Vol. PHP-10, pp. 101-109, 1974.

[3]. J.I. Smith, "The Even- and Odd-Mode Capacitance Parameters for Coupled Lines in Suspended Substrate", IEEE Transactions on Microwave Theory and Techniques, Vol. MTT-19, No. 5, May 1971, pp. 424-431.

[4]. R.A. Pucel, "Technology and Design Considerations of Monolithic Microwave Integrated Circuits", Published in Gallium Arsenide Technology, D.K. Ferry, Editor, Howard W. Sams & Co., Inc., 1985, pp. 225-230.

[5]. R.H. Jansen et al, "Theoretical and Experimental Broadband Characterisation of Multiturn Square Spiral inductors in Sandwich Type GaAs MMIC's", 15th European Microwave Conference, Digest of Technical Papers, Paris, Sept. 1985.